ORIGINAL ARTICLE

A novel inhibitor of N^6-methyladenosine demethylase FTO induces mRNA methylation and shows anti-cancer activities

Guoyou Xie[a,†], Xu-Nian Wu[a,†], Yuyi Ling[a,†], Yalan Rui[a,†], Deyan Wu[a], Jiawang Zhou[a], Jiexin Li[a], Shuibin Lin[c], Qin Peng[d], Zigang Li[d], Hongsheng Wang[a,d,*], Hai-Bin Luo[a,b,*]

[a]School of Pharmaceutical Sciences, Sun Yat-sen University, Guangzhou 510006, China
[b]Key Laboratory of Tropical Biological Resources of Ministry of Education, School of Life and Pharmaceutical Sciences, Hainan University, Haikou 570228, China
[c]Center for Translational Medicine, the First Affiliated Hospital, Sun Yat-sen University, Guangzhou 510080, China
[d]Institute of Systems and Physical Biology, Shenzhen Bay Laboratory, Shenzhen 518067, China

Abstract N^6-methyladenosine (m6A) modification is critical for mRNA splicing, nuclear export, stability and translation. Fat mass and obesity-associated protein (FTO), the first identified m6A demethylase, is critical for cancer progression. Herein, we developed small-molecule inhibitors of FTO by virtual screening, structural optimization, and bioassay. As a result, two FTO inhibitors namely 18077 and 18097 were identified, which can selectively inhibit demethylase activity of FTO. Specifically, 18097 bound to the active site of FTO and then inhibited cell cycle process and migration of cancer cells. In addition, 18097 reprogrammed the epi-transcriptome of breast cancer cells, particularly for genes related to P53 pathway. 18097 increased the abundance of m6A modification of suppressor of cytokine signaling 1 (*SOCS1*) mRNA, which recruited IGF2BP1 to increase mRNA stability of *SOCS1* and subsequently activated the P53 signaling pathway. Further, 18097 suppressed cellular lipogenesis *via* downregulation of peroxisome proliferator-activated receptor gamma (*PPARγ*), CCAAT/enhancer-binding protein alpha (*C/EBPα*), and *C/EBPβ*. Animal studies confirmed that 18097 can significantly suppress *in vivo* growth

*Corresponding authors. Tel./fax: +86 20 39943024 (Hongsheng Wang), +86 20 39943031 (Hai-Bing Luo).
E-mail addresses: whongsh@mail.sysu.edu.cn (Hongsheng Wang), hbluo@hainanu.edu.cn (Hai-Bin Luo).
†These authors made equal contributions to this work.

and lung colonization of breast cancer cells. Collectively, we identified that FTO can work as a potential drug target and the small-molecule inhibitor 18097 can serve as a potential agent against breast cancer.

1. Introduction

N^6-Methyladenosine (m^{6}A) is the most abundant modification of mRNA in eukaryote. It has been identified in the mid-1970s[1,2], accounting for approximately 50% of methylated ribonucleotides[3]. In mammalian cells, m^{6}A modification is demethylated by fat mass and obesity-associated protein (FTO)[4] and AlkB Homolog 5 (ALKBH5)[5]. While methyltransferase complex including methyltransferase like 3/14 (METTL3/14), WT1 associated protein (WTAP), RNA-binding motif protein 15 (RBM15)/15B and KIAA1429 is responsible for m^{6}A methylation[6]. The dynamic of m^{6}A is critical for mRNA splicing, nuclear export, stability and translation[7]. The m^{6}A methylation participates in various physiological processes, including embryonic development, stress responses and cell fate decision[7]. Accumulating evidence shows dysregulation of m^{6}A can induce pathogenesis of multiple diseases including cancers[8], which has prompted the development of therapeutic approaches to target this epigenetic machinery.

FTO is described as the first gene in association with common obesity[9]. In 2011, it has been firstly identified as a demethylase of mRNA m^{6}A in cell nucleus[4], which started the research boom of m^{6}A methylation and epitranscriptome. As a member of non-heme Fe^{II}/α-KG-dependent dioxygenase AlkB family protein, FTO prefers substrate of single-stranded nucleic acids[10]. Various previous studies have verified the *in vitro* and *in vivo* demethylation activities of m^{6}A of FTO[11–13]. Recent works suggested that FTO can act as an oncogenic factor and trigger the progression of various human cancers, such as leukemia[11,13], glioblastoma[14], melanoma[15], breast cancer[16] and renal clear cell carcinoma[17]. All these results suggested that FTO might be a potent target for drug development and cancer therapy.

Several studies tend to identify small-molecule inhibitors of FTO to intervene RNA methylation and cancer progression. Nowadays, several inhibitors such as rhein, MO-I-500, meclofenamic acid (MA), R-2HG, fluorescein, FB23-2 and entacapone have been reported to suppress the demethylation activities of FTO[11,18–24]. However, only few inhibitors showed cellular activities such as regulation of cell growth and/or proliferation[21]. Recently, CS1 and CS2 have been identified as potent FTO inhibitors to sensitize leukemia cells to T cell cytotoxicity[25]. It highlights the broad potential of targeting FTO for physiological dysregulations including cancer therapy. However, novel and highly effective inhibitors of FTO with high anti-cancer activities, particularly for solid tumors, are still urgently needed.

In the present study, a structure-based hierarchical virtual screening approach was used to identify novel FTO inhibitors. Subsequently, candidates were comprehensively validated by use of biochemical, cellular and *in vivo* experiments. We identified that a novel inhibitor, named as 18097, can specifically inhibit demethylation activity of FTO and then suppress cell migration, invasion, and lipogenesis of cancer cells.

2. Materials and methods

2.1. Virtual screening a selective compound of FTO

AutoMD, a MD-based virtual screening approach[26], was applied in the present study. AutoMD includes the establishment of pharmacophore model, molecular docking and dynamics simulations, and free energy prediction. Based on the crystal structures of FTO (Protein Data Bank, PDB ID: 4CXW, 4CXX, 4CXY, 4IE6, and 4ZS2), two binding sites in FTO were determined and two pharmacophore models were built. The commercial database SPECS (https://www.specs.net), which contains about 200,000 compounds, was selected for virtual screening through AutoMD. After molecular docking, 26 molecules were selected according to the proper binding patterns and high binding energies between ligands and FTO protein (Supporting Information Table S1).

2.2. Compound synthesis

The details for compound synthesis were described in the Supporting Information. Briefly, phthalic anhydride (1 mmol) and non-substituted or substituted resorcinol (2.2 mmol) were dissolved in methanesulfonic acid (1.5 mL). Subsequently, the mixture was stirred at 100 °C for 24 h. After cooling to room temperature, the mixture was poured into ice water and filtered. The solids were collected and dissolved in 4 mol/L sodium hydroxide solution, and then stirred for 30 min. Hydrochloric acid was added slowly under stirring until precipitation (pH < 5). The precipitate was collected and dried to yield the final product.

2.3. The restriction endonuclease digestion assay

The restriction endonuclease digestion assay was used to evaluate the *in vitro* demethylation activity of FTO and ALKBH5 according to the previous study[18]. Briefly, the 49 nt single-stranded DNA (ssDNA) substrate was synthesized and methylated as previously described[27]. A Dpn II cleavage site was included in ssDNA substrate. The 100 μL reaction mixtures including potential inhibitors were incubated at room temperature for 2 h. After quenching the reactions and ssDNA annealing, Dpn II was added to digest the non-methylated dsDNA. Digestion samples were loaded on 20% non-reducing PAGE. The band intensity was stained with GoldView™.

2.4. Circular dichroism (CD)

Chirascan CD spectrometer was used to record the CD of FTO with inhibitor candidates according to the previous study[18]. Measurements were taken in a 0.1 nm path length quartz cuvette at the wavelength rang of 200−250 nm at 25 °C. Before CD analysis, the FTO protein (5 μmol/L in 20 mmol/L sodium phosphate, pH

8.0) made in our lab was incubated with inhibitor candidates 18097/18077 for 1 h at 25 °C.

2.5. Cell culture and transfection

Human cancer cells including MDA-MB-231, HeLa, HEK-293T, A549, A375 and mouse 3T3-L1 cells were cultured in RPMI-1640 medium or DMEM (GIBCO, Carlsbad, CA, USA) supplemented with 10% fetal bovine serum (FBS) at 37 °C in 5% CO_2. MycoAlert Mycoplasma Detection Kit was routinely used to test mycoplasma contamination.

Three synthesized duplex RNAi oligos targeting human suppressor of cytokine signaling 1 (*SOCS1*), FTO, or insulin like growth factor 2 mRNA binding protein 1 (*IGF2BP1*) mRNA sequences (Sigma), respectively, were used. The RNA negative control (si-NC, 5′-UUCUCCGAACGUGUCACGU) and siRNAs (working concentration 50 nmol/L) were transfected by use of lipofectamine RNAiMAX (Invitrogen) following the product instruction. After measured the knockdown efficiency, the most efficient oligo was used for next investigations.

2.6. Fluorescence polarization (FP) assay

The FP assay was conducted according to the previous study[18]. Briefly, 50 nmol/L compound 18097 and varying concentrations of FTO were incubated in 100 μL 50 mmol/L borate buffer, pH
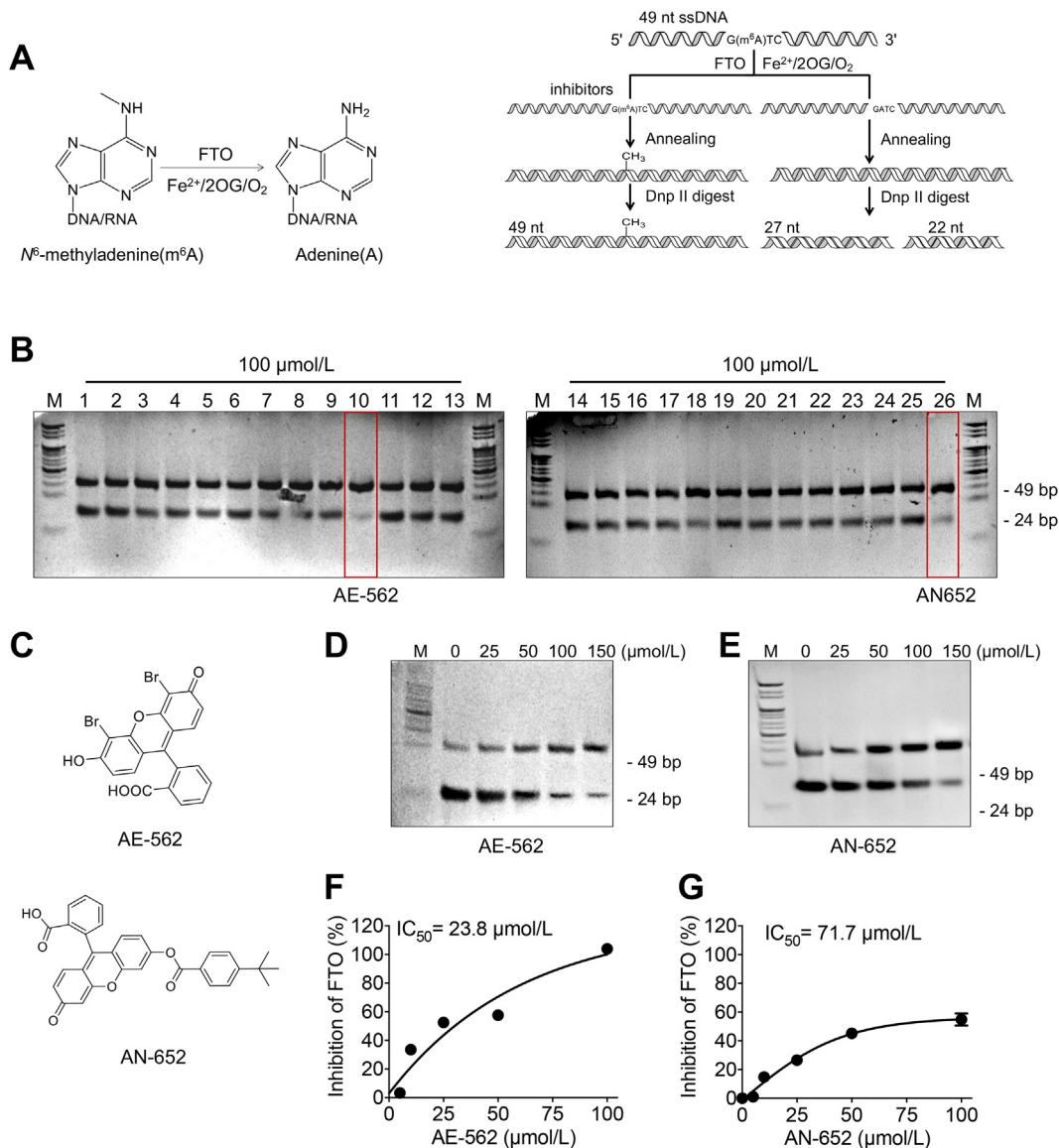

Figure 1 AE-562 and AN-652 were potential FTO inhibitors. (A) The schematic diagram of restriction endonuclease digestion assay to test activities of potential FTO inhibitors. (B) The restriction endonuclease digestion assay for the inhibition effects of 26 compounds from virtual screening. The upper band represents the full-length dsDNA (49-mer) containing m^{6}A modification. The lower band is the mixtures of 22- and 27-mer dsDNA after DpnII digestion. The disappear of the lower band suggests the inhibition of FTO. (C) Structures of AE-562 and AN-652 which can potentially inhibit activity of FTO; (D) and (E) The restriction endonuclease digestion assay for increasing concentrations of AE-562 (D) and AN-652 (E). The results showed that AE-562 and AN-652 can inhibit *in vitro* demethylation activity of FTO *via* a concentration-dependent manner; (F) and (G) The effects of AE-562 (F) and AN-652 (G) on *in vitro* demethylation efficiency of FTO were quantitatively analyzed by using HPLC−MS/MS. The IC$_{50}$ values of AE-562 and AN-652 are 23.8 and 71.7 μmol/L, respectively.

7.5 for 30min at 25 °C. FP was then measured by fluorescence spectrophotometer (Fluoromax-4, HORIBA, American). The wavelengths for excitation and emission were 480 and 520 nm, respectively. GraphPad prism 5.0 was used to calculate binding parameters between FTO and compound.

2.7. Cell proliferation assay and colonization assay

The Cell Counting Kit-8 (CCK-8) (Dojindo Molecular Technologies) was used to test effects of compound 18077 and 18097 on cell proliferation according to our previous study[28]. CytoSelect 96-well Cell Transformation Assay (Cell Biolabs, USA) was used to check effects of compound 18077 and 18097 on colony formation following the product instruction.

2.8. RNA-seq and GESA analysis

MDA-MB-231 cells were treated with or without 100 μmol/L 18097 for 24 h. Total RNAs were purified by use of RNeasy mini

kit (Qiagen, Germany). NuGEN Ovation RNA-Seq Systemv2 (NuGEN, San Carlos, CA) was used for reverse transcription. The mRNA-seq was conducted as reported previously[29]. The reads were mapped to human genome sequence (NCBI 36.1 [hg19]) by use of TopHat (version 2.0.6). R/Bioconductor package edgeR (version 3.0.8) was used to evaluate the difference of gene expression. FDR of <0.05 and >200 bp of genes were defined as differentially expressed and listed at Supporting Information Table S2. For gene set enrichment analysis (GSEA) analysis, standard procedures as described by GSEA user guide (http://www.broadinstitute.org/gsea/doc/GSEAUserGuideFrame.html) were used. Curated gene set C2 of the Molecular Signature Database version 4.0 was used to analyze the overlaps between our gene set and gene sets in Molecular Signature Database.

2.9. RNA-extraction and qRT-PCR

RNA extraction and qRT-PCR were described in our previous study[30]. The primers used in the present study are listed at
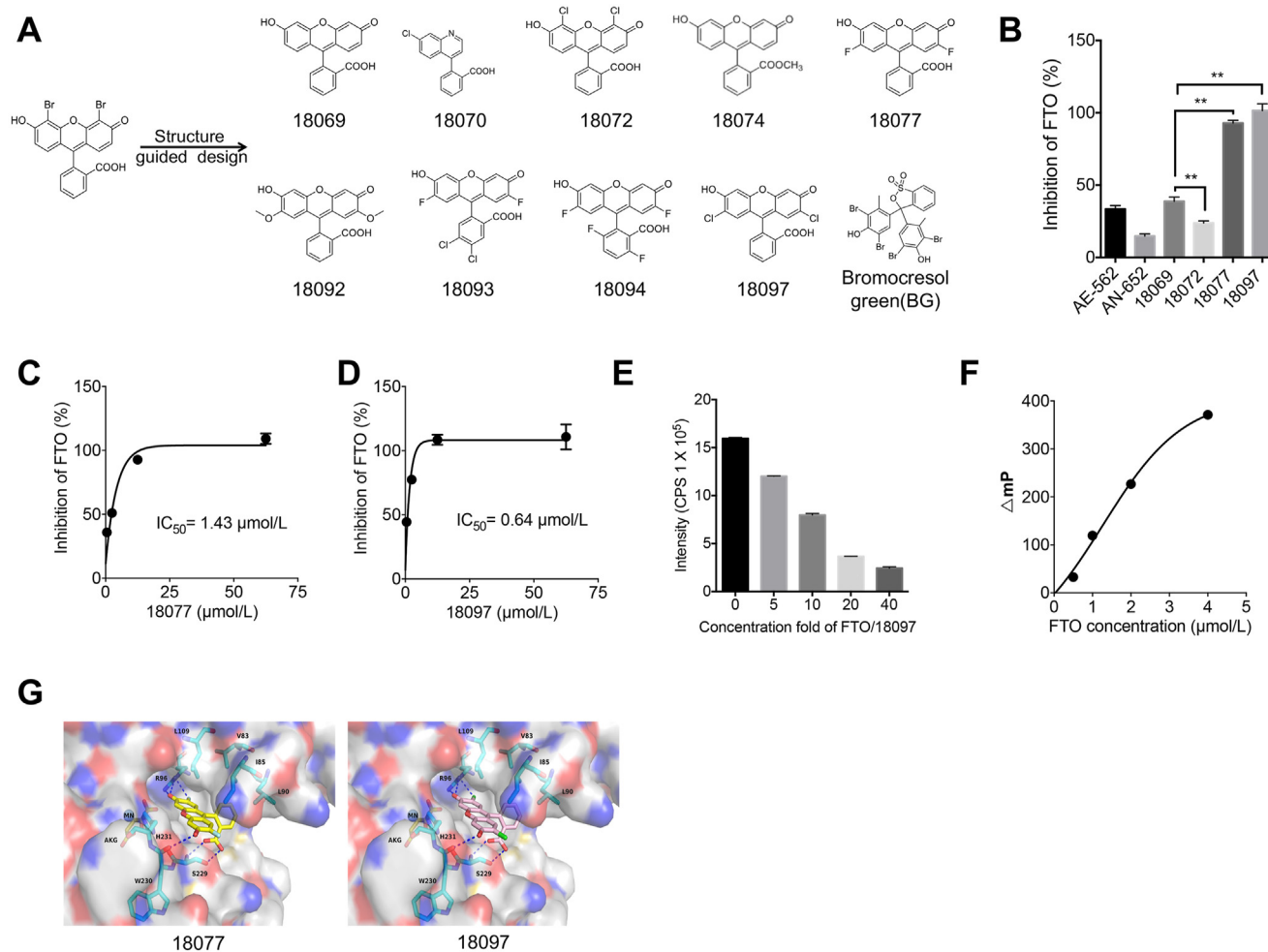

Figure 2 The structural optimization of FTO inhibitors and their characteristics. (A) The structure-based design of potential inhibitors. 6-Hydroxy-3H-xanthen-3-one compounds as the key element of compound to guide structure-based design. (B) The inhibitory effects of potential inhibitors (10 μmol/L) on FTO were analyzed by use of HPLC/MS/MS. (C) and (D) Effects of 18077 (C) or 18097 (D) on in vitro demethylation activities of FTO was quantified by HPLC−MS/MS. The IC$_{50}$ values of 18077 and 18097 are 1.43 and 0.64 μmol/L, respectively. (E) The fluorescence intensity of 18097 incubated with increasing concentrations of FTO in the reaction system, indicating that 18097 can directly target FTO. (F) The fluorescence polarization (FP) assay for displacement of small-molecule inhibitors binding to FTO, which confirmed that 18097 is a selective and potent inhibitor of FTO. (G) In silico analysis for binding of 18077/18097 with the active stie of FTO. Data represent as means ± SD, $n = 3$, **$P < 0.01$.

Supporting Information Table S3. The expression of targeted transcripts was calculated using $2^{-\Delta\Delta CT}$ method with GAPDH as the internal control.

2.10. RIP-RT-PCR

The RIP-RT-PCR was conducted as described in our previous study[31]. Briefly, two 10-cm plates of cells were washed by cold PBS and then lysed by use of 400 μL IP lysis buffer on ice for 30 min. Clear lysate was collected after $12,000 \times g$ centrifugation for 10 min. 4 μL targeted antibodies or IgG (NEB, USA) were pre-coated on magnetic beads for 2 h. The antibody-coated beads were incubated with clear cell lysate at 4 °C overnight. Proteinase K was added to digest proteins in the immunoprecipitated RNA-protein complex, followed by TRIzol extraction of precipitated RNAs. The interested RNAs were detected by RT-qPCR and normalized to input.

2.11. Experimental animals and xenograft models

Animal experiments were conducted according to the requirements of Zhongshan School of Medicine Policy on the Care and Use of Laboratory Animals. Two cohorts of animal studies were performed in the present study. Firstly, subcutaneous transplanted model was used to evaluate the growth of breast cancer cells. The immunodeficient female mice were subcutaneously injected with cells (MDA-MB-231, 5×10^6 per mouse) resuspended in 200 μL PBS plus 200 μL matrigel (BD Biosciences). Mice were randomly divided into two groups ($n = 6$ for each group) when their tumor volumes reached approximately 100 mm³. The compound 18097 group was administrated with 18097 (50 mg/kg) every day by i.p. injection. The control group was administrated with equal volume of PBS. The tumor volume was recorded every day and calculated by Eq. (1):

$$V = 1/2 \times D_{\text{larger}} \times D_{\text{smaller}}^2 \tag{1}$$

where D represent diameter. All mice were euthanized when volumes of tumors in the control group are around 1000 mm³. Tumors were removed to measure the expression of Ki-67, SOCS1, and PPARγ by IHC.

For lung metastatic (LM) model, the establishment of lung metastasis of breast cancer (BC) cell model was described in our previous studies[28,31]. In brief, the first generation of LM cells were obtained from the lung of immunodeficient mice (four weeks old) after injecting with 2×10^5 viable cells (MDA-MB-231, 100 μL) into the lateral tail vein. Eight weeks later, the lung metastasized cells were isolated, primarily cultured with medium supplemented with 10% FBS, and named as MDA-MB-231$^{\text{LMF1}}$. The LMF2 and LMF3 BC cells were generated by use of the same method. The MDA-MB-231$^{\text{LMF3}}$ cells (7×10^5 per mouse, 2 groups, $n = 8$ for each group) were resuspended in 50 μL base medium, followed by tail vein injection. After two weeks, the mice were intraperitoneally injected with 18097 (50 mg/kg) or saline for 16 days. The experiment was terminated after eight weeks of injection, then mice were sacrificed and lungs were isolated and analyzed for the presence of metastatic tumours.

2.12. Statistical analysis

Results were described as mean ± standard deviation (SD) from three independent experiments unless otherwise specified. Two-tailed unpaired Student's t-test was used to analyze the difference between two groups, and One-Way ANOVA followed by Bonferroni test was used for multiple comparison. The statistical analyses were performed using SPSS 17.0 for Windows. A P-value of <0.05 was considered as statistically significant; $^*P<0.05$, $^{**}P<0.01$. NS, no significant.

3. Results

3.1. AE-562 and AN-652 were potential inhibitors of FTO

To discover potential FTO inhibitors, we designed a combining computational (namely AutoMD)[32] and experimental method, which contained pharmacophore model, molecular docking and dynamics simulations, free energy prediction, and bioassay (Supporting Information Fig. S1A). The crystal structures of FTO (PDB code 4CXW, 4CXX, 4CXY, 4IE6, and 4ZS2) were used as pharmacophore models for *in silico* analysis by use of more than 200,000 molecules in the SPECS database (Fig. S1B). On the basis of both appropriate binding patterns and top-ranked predicted binding energies, 26 compounds were ordered from SPECS for the subsequent bioassay (Table S1).

As shown in Fig. 1 A, the restriction endonuclease digestion assay by use of 49-mer ssDNA was used to validate potential inhibitors as previously reported[18,27]. To confirm the efficiency of method, we incubated substrate with FTO protein for increasing time periods. The data showed that FTO can rapidly (15 min) demethylate m⁶A methylated 49-mer ssDNA. This effect reached the highest after incubation for 2 h (Fig. S1C). We further incubated substrate with different concentrations of FTO for 2 h. The results showed that 0.5 μmol/L FTO can effectively demethylate m⁶A methylated 49-mer ssDNA in the reaction system (Fig. S1D).

Then, the inhibition effects of 26 compounds from virtual screening were evaluated by the restriction endonuclease digestion assay. Results indicated that AE-562 and AN-652 showed the highest inhibition effects among all tested 26 compounds (Fig. 1B and C). Further, restriction endonuclease digestion assay showed that both AE-562 (Fig. 1D) and AN-652 (Fig. 1E) can inhibit the *in vitro* demethylation activity of FTO *via* a concentration dependent manner. The standard curve (Fig. S1E) was established *via* normalization the response area to m⁶A standards by use of HPLC−MS/MS according to our previous study[31]. We then quantitatively analyzed the inhibition effects of potential inhibitors. The results showed that both AE-562 (Fig. 1F) and AN-652 (Fig. 1G) can dose dependently inhibit the demethylation activity of FTO with IC_{50} values of 23.8 and 71.7 μmol/L, respectively. Treatment with AE-562 and AN-652 can significantly increase mRNA m⁶A in HeLa cells (Fig. S1F). These data indicated that these two compounds are potential FTO inhibitors.

3.2. The optimization of FTO inhibitors and their characteristics

Since AE-562 and AN-652 showed common structural scaffold (Fig. 2A) targeting FTO (Supporting Information Fig. S2A), we further optimized the hits to increase inhibition potency of FTO demethylation. The scaffold shared by AE-562 and AN-652, 2-(6-hydroxy-3-oxo-3H-xanthen-9-yl) benzoic acid (18069), was synthesized. Results showed that 18069 had greater inhibitory capabilities than that of AE-562 or AN-652 on demethylation activity of FTO (Fig. 2B), implying that the large substituents at 4, 5, and/or 6 positions of the 6-hydroxy-3H-xanthen-3-one core might weaken the binding affinity. Replacement of hydrogen atoms by

chlorine atoms at 4, 5 positions on the 6-hydroxy-3*H*-xanthen-3-one core caused decrease in inhibitory activity as well (18072 *vs*. 18069, Fig. 2B).

To design more potent FTO inhibitors, halogen atoms were introduced at 2, 7 positions on the 6-hydroxy-3*H*-xanthen-3-one core based on the predicted binding modes (Fig. 2A). Finally, 18077 and 18097 were obtained and showed significantly upregulated activity to inhibit demethylation effect of FTO (Fig. 2B). Restriction endonuclease digestion assay showed that all optimized potential inhibitors can inhibit the *in vitro* demethylation activity of FTO *via* a concentration dependent manner (Fig. S2B).

HPLC−MS/MS showed that 18077 and 18097 were much more potent than AE-562 and AN-652 (Fig. 2B), with IC_{50} values of 1.43 µmol/L (Fig. C) and 0.64 µmol/L (Fig. 2D), respectively.

We then analyzed the binding between FTO and its potential inhibitors. The CD analysis showed that both 18077 (Fig. S2C) and 18097 (Fig. S2D) less than 200 µmol/L had no significant effect on FTO conformation. It indicated that the activity of inhibitors might not be due to induce conformation change of FTO. We then tested whether the inhibitor can directly interact with FTO. Fluorescence intensity assay showed that incubation with FTO can dose-dependently decrease fluorescence intensity of
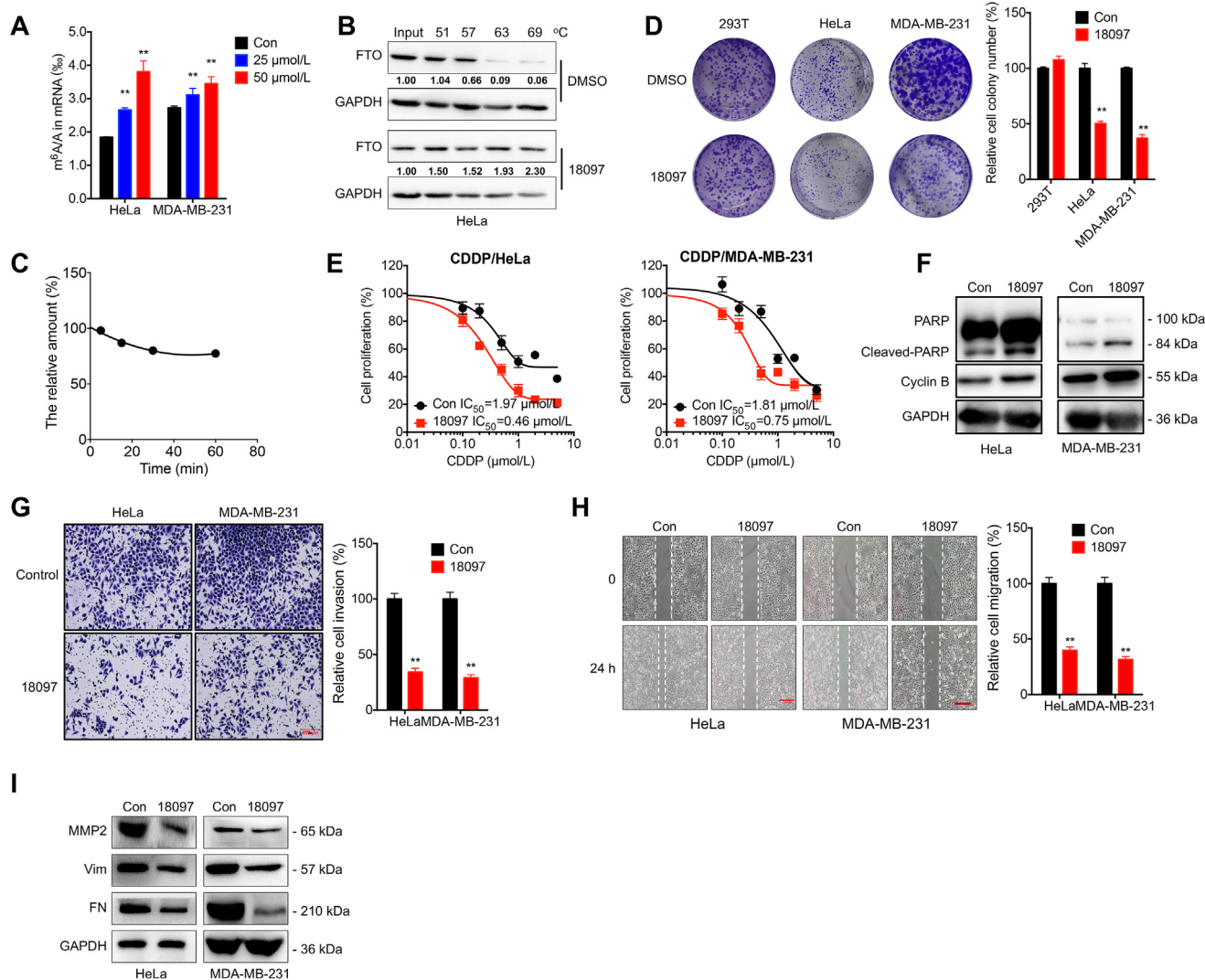

Figure 3 The FTO inhibitors suppressed malignancy of cancer cells. (A) Cells were incubated with or without FTO inhibitor 18097 for 24 h. The m[6]A in mRNA was checked using HPLC−MS/MS. (B) HeLa cells were incubated with or without 50 µmol/L 18097 to test the thermal stabilization of FTO protein; 18097 can increase the thermal stability of FTO. (C) The *in vitro* stability of 18097 was checked by use of rat liver microsome. Results indicated that the $t_{1/2}$ of 18097 was 250 min. (D) The colonization of 293T, HeLa, MDA-MB-231 cells treated with or without 50 µmol/L 18097, showing that 18097 significantly inhibited the capability of cell clone formation. (E) HeLa or MDA-MB-231 were pre-treated with 100 µmol/L 18097 for 6 h, and further incubated with increasing concentrations of CDDP for 24 h. Cell proliferation was then checked by CCK-8 kit. (F) Expression of PARP and cyclin B were increased in cells treated with 100 µmol/L 18097 for 24 h. (G) The invasion of HeLa and MDA-MB-231 cells treated with or without 50 µmol/L 18097 for 24 h, showing that 18097 significantly inhibited the capability of cells invasion. (H) The migration of HeLa and MDA-MB-231 cells treated with or without 50 µmol/L 18097 for 24 h, indicating that 18097 significantly inhibited the capability of cells migration. (I) The expression of MMP2, Vim and FN were decreased in cells treated with 50 µmol/L 18097 for 24 h. Data represent as means ± SD, $n = 3$, **$P < 0.01$.

18097 (Fig. 2E), indicating that 18097 can directly target FTO. FP assay was conducted to test the ability of the small-molecule inhibitors binding with FTO. Results showed that FTO can increase the ΔmP of 18097 *via* a concentration dependent manner (Fig. 2F), which confirmed that 18097 is a potent inhibitor of FTO. To verify that 18097 can directly inhibit FTO activity rather than chelation of Fe^{2+} during the *in vitro* assay, results showed that extra supplementary Fe^{2+} with concentrations even as high as 840 µmol/L, a 3-fold molar excess of Fe^{2+} with respect to the inhibitor, had no effect on inhibition effect of 18097 (Fig. S2E). It

indicated that 18097 can directly target FTO rather than chelate Fe^{2+} ion in solution.

Molecular modeling studies confirmed that 18077 and 18097 occupied the substrate binding site of FTO rather than the cofactor binding site (Fig. 2G), which were similar with the binding pattern of the fluorescein−FTO complex[23]. 18077/18097 formed H-bonding interactions with the residues Arg96, Ser299 and Trp230. A halogen atom (F or Cl in 18077 and 18097) contributed to the contact with the guanidinium group in Arg96 through hydrogen bonding, which enhanced binding affinity of compounds with
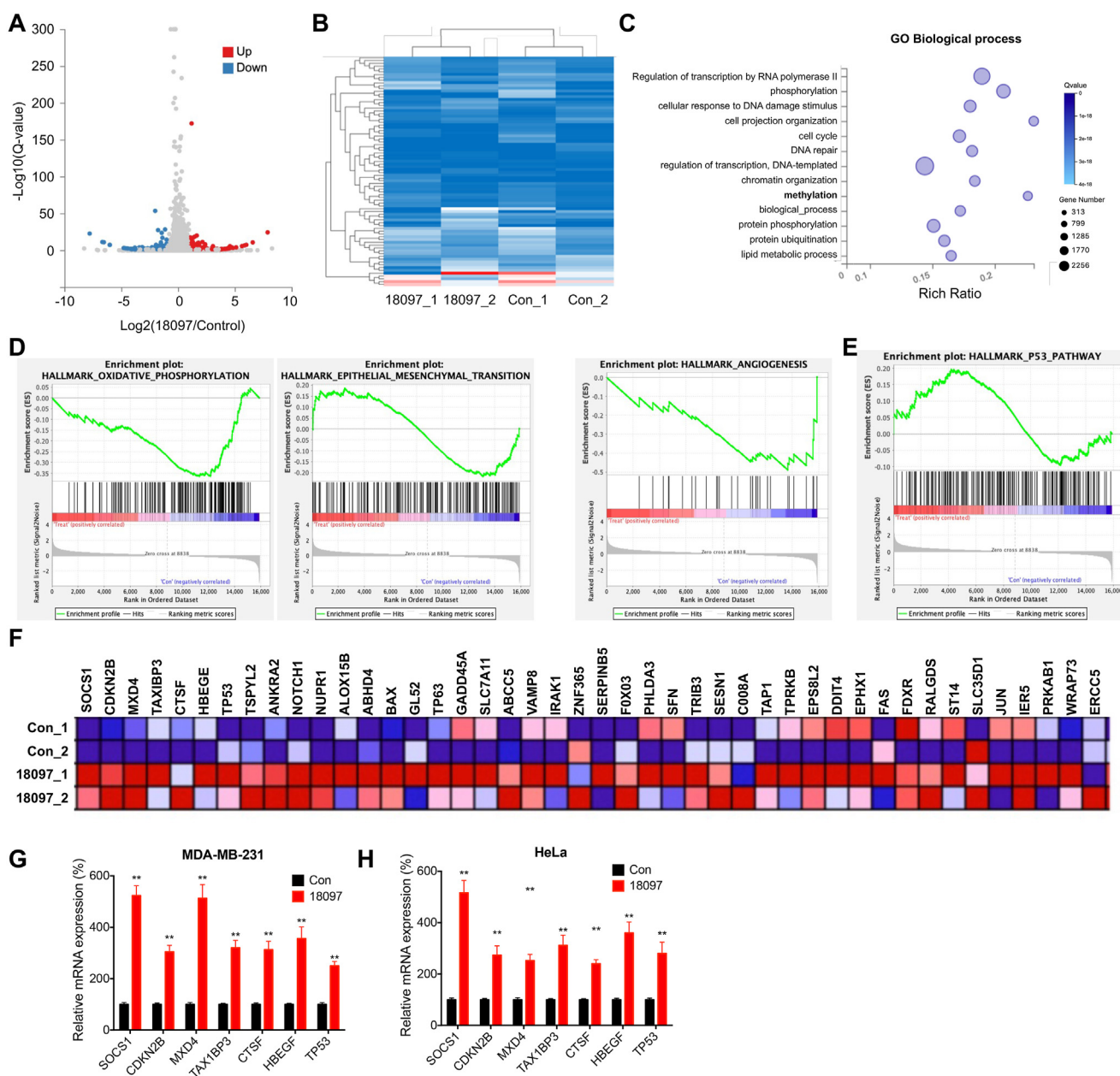

Figure 4 Modulation of transcriptome and genes involved in P53 pathway by 18097 treatment. (A) Volcano plots show genes of MDA-MB-231 cells treated with or without 18097 for 24 h. (B) Heatmap displays the overview of the differentially expressed genes after 18097 treatments. (C) Gene ontology categorization of biological process for assembled unigenes of the transcriptome induced by 18097 treatments. (D) GSEA analysis shows negative enrichment of 18097-altered genes in oxidative phosphorylation, epithelial mesenchymal transition, and angiogenesis. (E) GSEA analysis shows positive enrichment of 18097-altered genes in P53 pathway. (F) The significantly variated genes involved in P53 pathway in cells treated with 18097 for 24 h; (G) and (H) The mRNA expression of *SOCS1*, *CDKN2B*, *MXD4*, *TAX1BP3*, *CTSF*, *TP53* was significantly increased in MDA-MB-231 (G) and HeLa (H) cells treated with 18097 for 24 h. Data represent as means $\pm$ SD, $n = 3$, **$P < 0.01$.
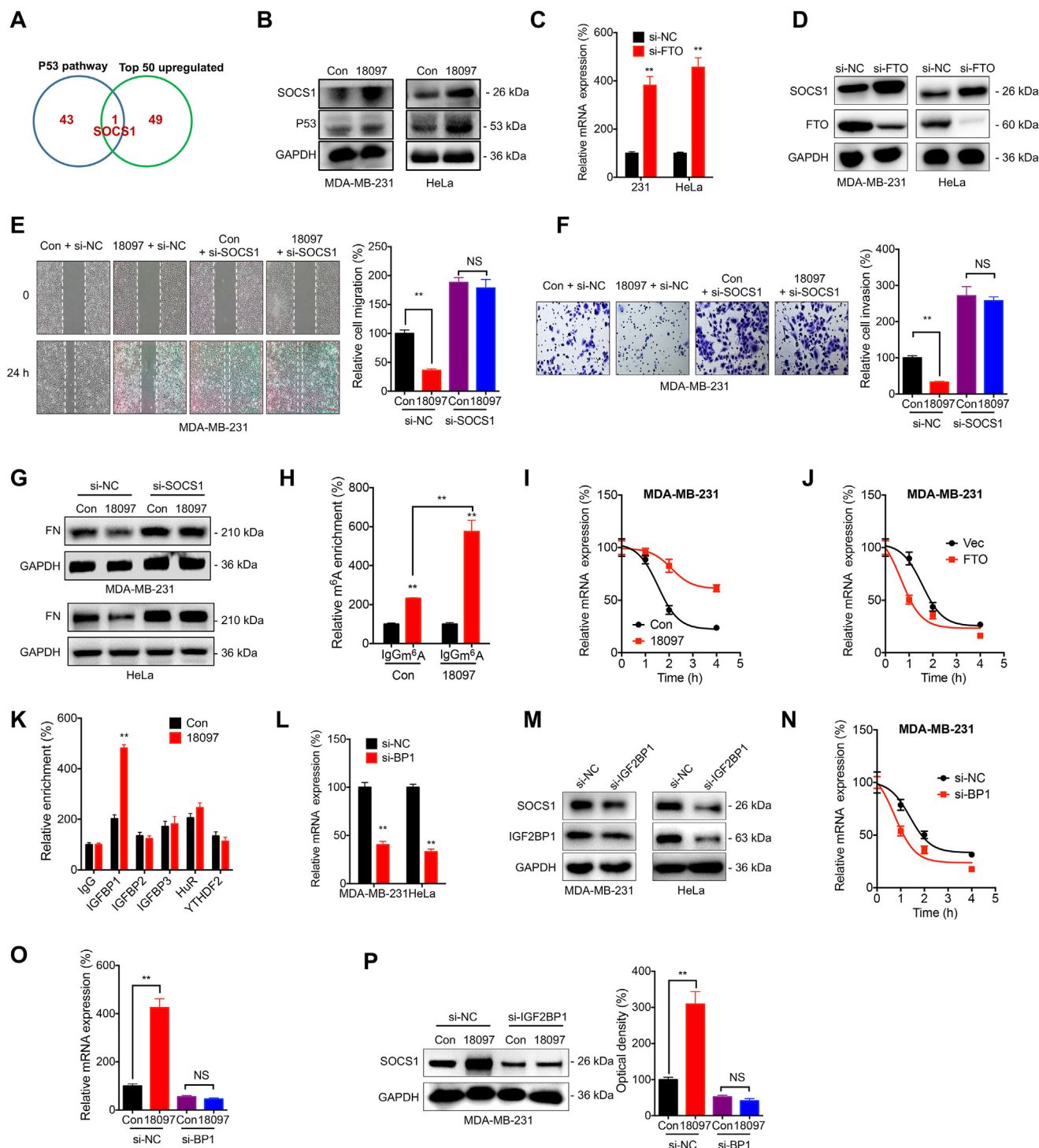
Figure 5 SOCS1 was involved in 18097-suppressed malignancy of cancer cells. (A) Venn diagram shows substantial and significant overlap among P53 pathway genes, and the top 50 up-regulated genes in MDA-MB-231 cells treated with 18097 compared with control cells. (B) The expression of SOCS1 and P53 was increased in cells treated with 100 μmol/L 18097 for 24 h. (C) and (D) Cells were transfected with si-NC or si-*FTO* for 24 h, the mRNA (C) and protein (D) expression of SOCS1 were checked; (E) and (F) MDA-MB-231 cells were transfected with si-NC or si-*SOCS1* for 12 h, followed by treatment with 100 μmol/L 18097 for 24 h. The migration (E) and invasion (F) of cells were detected. It showed that si-*SOCS1* can abolish 18097-suppressed migration and invasion. (G) Cells were transfected with si-NC or si-*SOCS1* for 12 h, followed by treatment with 100 μmol/L 18097 for 24 h. si-*SOCS1* abolished 18097-suppressed expression of FN in cancer cells. (H) m⁶A of *SOCS1* mRNA in cells treated with or without 100 μmol/L 18097 for 24 h was detected by m⁶A-RIP-PCR. 18097 increased m⁶A enrichment of *SOCS1* mRNA. (I) The mRNA level of *SOCS1* in MDA-MB-231 cells treated with or without 100 μmol/L 18097 for 24 h and further incubated with Act-D for 0–4 h, showing that 18097 significantly increased mRNA stability of *SOCS1*. (J) The mRNA level of *SOCS1* in MDA-MB-231 cells pre-transfected with vector or FTO constructs for 24 h and further incubated with Act-D for 0–4 h. (K) The relative enrichment of *SOCS1* in IGF2BP1−3, HuR, and YTHDF2 in MDA-MB-231 pre-treated with or without 100 μmol/L 18097 for 24 h were checked by RIP-qPCR analysis.
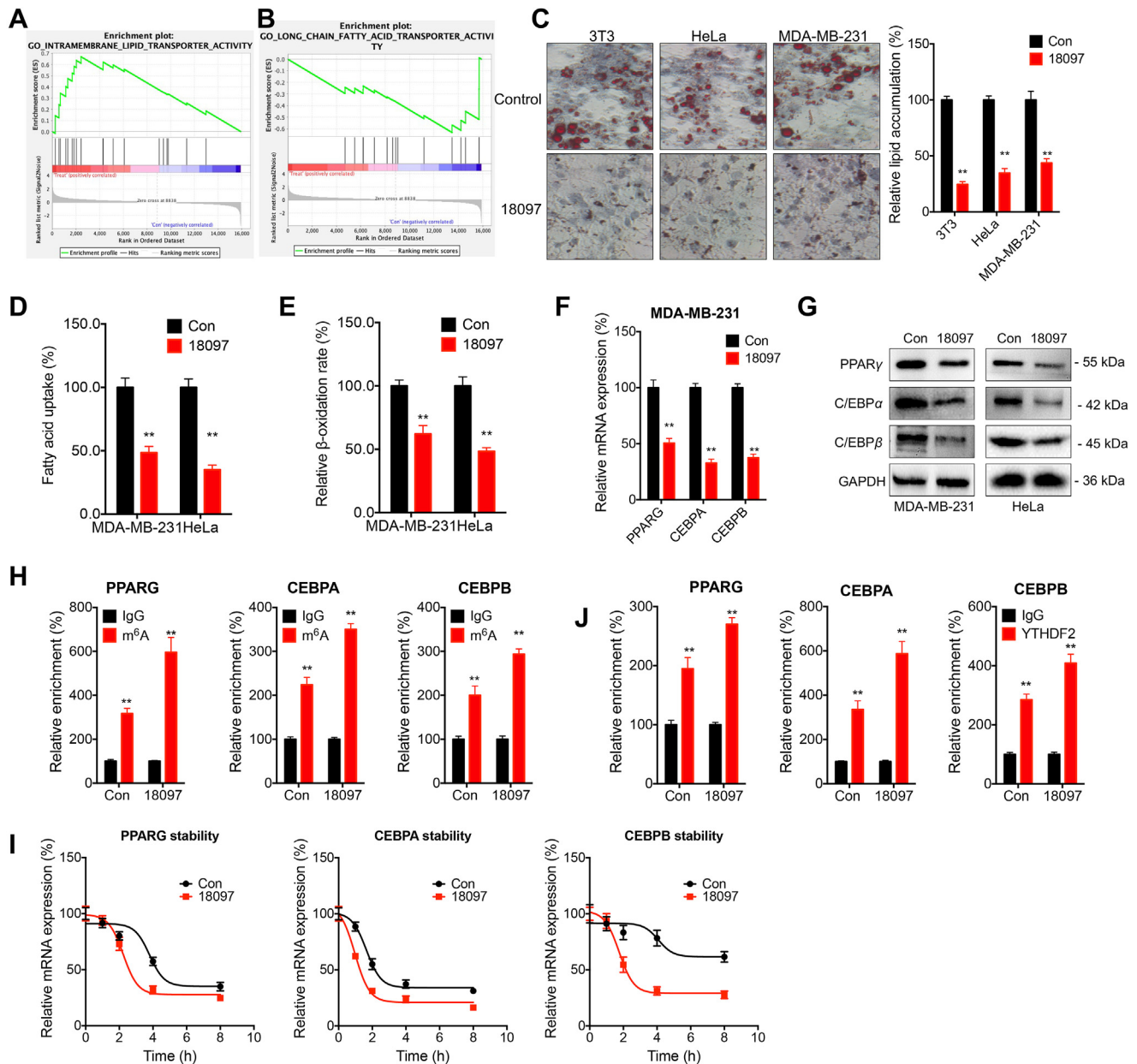
Figure 6 FTO inhibitor suppressed cellular lipogenesis. (A) GSEA analysis revealed positive enrichment of 18097-altered genes in GO_intramembrane lipid transporter activity. (B) GSEA analysis revealed negative enrichment of 18097-altered genes in GO_long chain fatty acid transporter activity. (C) Oil Red O (ORO) staining of the adipocytes from 3T3, HeLa, MDA-MB-231 cells incubated with or without 100 μmol/L 18097, indicating that 18097 significantly decreased the neutral lipid accumulation. (D) and (E) The relative fatty acid uptake (D) and β-oxidation rate (E) in cells incubated with or without 100 μmol/L 18097 for 24 h, showing that treatment with 18097 can significantly suppress the fatty acid (FA) uptake and FAO rate of cancer cells. (F) The mRNA expression of *PPARG*, *CEBPA*, and *CEBPB* were decreased in MDA-MB-231 cells incubated with 100 μmol/L 18097 for 24 h. (G) The protein expression of PPARγ, C/EBPα, and C/EBPβ were decreased in MDA-MB-231 and HeLa cells incubated with 100 μmol/L 18097 for 24 h. (H) The relative m^6A levels of *PPARG*, *CEBPA*, and *CEBPB* in MDA-MB-231 cells incubated with 100 μmol/L 18097 for 24 h were checked by m^6A-RIP-PCR. (I) MDA-MB-231 cells were pretreated with or without 100 μmol/L 18097 for 24 h, and then were incubated with Act-D for 0−8 h. The mRNA levels of *PPARG*, *CEBPA*, and *CEBPB* were checked; (J) MDA-MB-231 cells treated with or without 100 μmol/L 18097 for 24 h. The interaction between YTHDF2 and mRNA were analyzed by RIP-PCR. Data represent as means ± SD, $n = 3$, **$P < 0.01$.

(L) The mRNA level of *SOCS1* was decreased in cells transfected with si-*IGF2BP1* for 24 h. (M) Protein expression of SOCS1 and IGF2BP1 were decreased in cells transfected with si-*IGF2BP1* for 24 h. (N) The mRNA level of *SOCS1* in MDA-MB-231 cells transfected with si-NC or si-*IGF2BP1* constructs for 24 h and then incubated with Act-D for 0−4 h. (O) and (P) Cells were transfected with si-NC or si-*IGF2BP1* constructs for 12 h, and then incubated with or without 100 μmol/L 18097 for 24 h. The mRNA (O) and protein (P) expression of SOCS1 were checked. Data represent as means ± SD, $n = 3$, **$P < 0.01$.
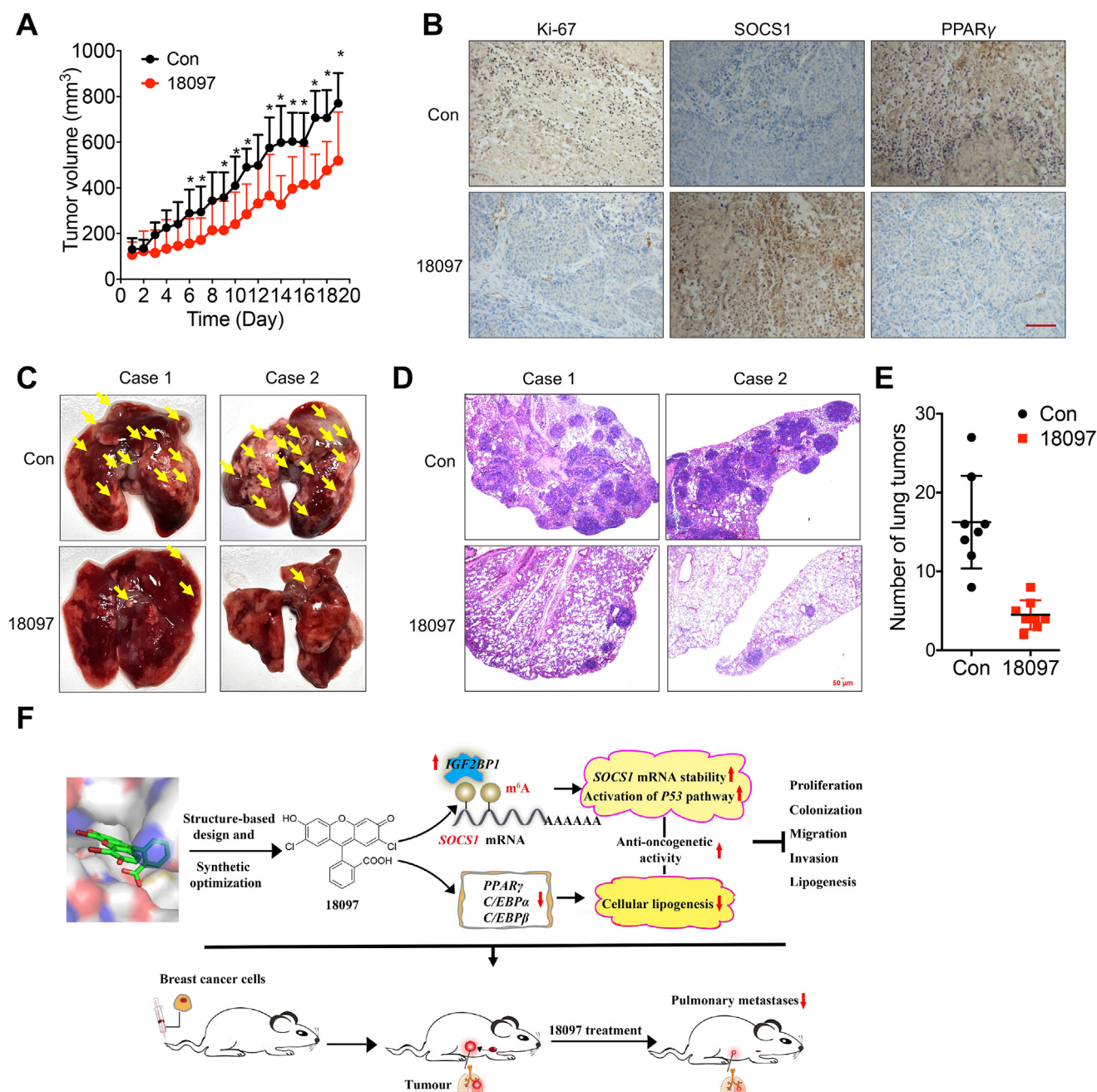
Figure 7 Effects of FTO and its inhibitor on *in vivo* progression of breast cancer. (A) The tumor volumes of control and 18097 group were recorded in MDA-MB-231 xenograft models ($n=6$ for each group), showing that injecting 18097 significantly suppressed tumor growth; (B) IHC-stained sections from control and 18097 group of MDA-MB-231 xenografts; (C)−(E) Cells were injected *via* tail vein into the nude mice ($n=8$ for each group), and the metastatic lung tumors were isolated. Representative images of metastatic lung tumors were shown (C) and (D). The number of lung tumors were quantitatively recorded (E). (F) Proposed model to illustrate the development of FTO inhibitor 18097 and its anti-cancer activities. Data represent as means ± SD, *$P < 0.05$.

FTO. Besides, the phenyl ring in 18077/18097 made hydrophobic interactions with the FTO nucleotide recognition lid (NRL) mainly composed by Val83, Ile85, Leu90 and Leu109, which is proposed to improve the selectivity of potential inhibitors.

We further evaluated the enzyme selectivity of potential inhibitors *via* examination its activity against ALKBH5, the other mammalian RNA m6A demethylase[5]. Results showed that even

the concentration as high as 100 μmol/L, potential inhibitors had no distinct effect on ALKBH5-mediated m6A conversion (Fig. S2F). Further, HPLC−MS/MS showed that IC$_{50}$ value of 18097, the most potent FTO inhibitor, was 179 μmol/L for ALKBH5 (Fig. S2G), which is about 280-fold greater than that to FTO. It suggested that the identified inhibitors can selectively suppress FTO activity.

3.3. The FTO inhibitor showed anti-cancer activities

We further checked cellular activities of FTO inhibitor 18097 since it had the greatest *in vitro* inhibition effect to FTO. The results showed that 18097 can significantly increase mRNA m^{6}A methylation in HeLa and MDA-MB-231 cells with the percentage of 44.10% and 14.23% at 25 μmol/L, and percentage of 106.67% and 26.66% at 50 μmol/L, respectively (Fig. 3A). Further, cellular thermal shift assay (CESTA) showed that treatment with 18097 can significantly increase protein stability of FTO in both HeLa (Fig. 3B) and MDA-MB-231 cells (Supporting Information Fig. S3A). The rat liver microsome assay was used to test the *in vitro* hepatic stability of 18097. Results indicated that 18097 was not almost metabolized by rat liver microsome (Fig. 3C).

We further tested effects of inhibitor on clone formation of both human renal epithelium (293T) and cancer cells. The results showed that 18097 had no significant effect on clone formation of 293T cells, while significantly ($P<0.05$) suppressed colony number of various cancer cells including cervical HeLa, breast cancer MDA-MB-231, lung cancer A549, and melanoma A375 cells (Fig. 3D and Fig. S3B). Further, treatment with 18097 can increase cisplatin (CDDP) sensitivity of HeLa and MDA-MB-231 cells (Fig. 3E). Consistently, treatment with 18097 also increased doxorubicin (Dox) sensitivity of HeLa and MDA-MB-231 cells (Fig. S3C). We further checked potential effects of inhibitor on cell cycle and apoptosis of cancer cells. Data showed that treatment with 18097 can increase proportions of G0/G1 of cancer cells while decrease percentage of G2/M cells of HeLa cells (Fig. S3D). In addition, 18097 can induce cell apoptosis (Fig. S3E) and expression of cleaved-PARP and cyclin B in checked cells (Fig. 3F). It suggested that 18097 can suppress proliferation and increase chemosensitivity of cancer cells.

In addition, 18907 can significantly inhibit *in vitro* invasion capability of cancer cells (Fig. 3G). Wound healing assay showed that 18907 can suppress migration of HeLa and MDA-MB-231 cells (Fig. 3H). Western blot analysis confirmed that 18097 can suppress expression of matrix metallopeptidase 2 (MMP2), fibronectin (FN) and vimentin, the well-known mesenchymal markers of cancer cells (Fig. 3I). It indicated that 18097 can suppress migration, invasion and epithelial−mesenchymal transition (EMT) of cancer cells.

3.4. Modulation of transcriptome and genes involved in P53 pathway by 18097 treatment

We then tested effect of the FTO inhibitor on transcriptome. The expression levels of 302 genes were significantly changed with the upregulation of 168 and down regulation of 134 genes in cells treated with 18097 (Fig. 4A). Individually sequenced transcriptomes and differentially expressed genes from control and 18097 group are indicated in Fig. 4B. Gene ontology (GO) classes indicated that gene categories including methylation (Fig. 4C), methyltransferase activity (Supporting Information Fig. S4A), and cellular component (Fig. S4B) exhibited significant overall changes in 18097 group. The different genes were further analyzed by Kyoto Encyclopedia of Genes and Genomes (KEGG) pathway annotation[33], which indicated that key pathways for cancer progression including metabolism of xenobiotics, metabolic pathways was regulated by 18097 (Fig. S4C).

Results of GSEA revealed that the gene expression profile induced by 18097 treatment was negatively associated with oxidative phosphorylation, EMT, angiogenesis and estrogen response of MDA-MB-231 cells (Fig. 4D and Fig. S4D), suggesting that 18097 may suppress cancer progression *via* inhibiting the metabolic, EMT and angiogenesis. Further, treatment of 18097 decreased the gene sets of ribosome, proteasome, fructose and mannose metabolism in MDA-MB-231 cells (Fig. S4E), which might impair RNA translation, protein degradation and trigger cancer death. Collectively, RNA-seq data revealed that treatment of 18097 altered a handful of genes related to cell metabolism, EMT and cell malignancy.

We further characterized potential pathways involved in 18097-suppressed malignancy of cancer cells *via* GESA analysis using hallmark gene sets. Our data showed that among the 50 hallmark gene sets, gene expression profile with 18097 treatment was positively associated with P53 (Fig. 4E) while negatively associated with Myc target (Fig. S4F) pathways. mRNA-seq revealed that treatment with 18097 increased the expression of 44 genes involved in P53 pathways (Fig. 4F) while decreased 96 genes involved in Myc targets (Fig. S4G). qPCR confirmed that treatment with 18097 significantly increased mRNA expression of *SOCS1*, *CDKN2B*, *TAX1BP3*, *CTSF*, *HBEGF* and *TP53* expression in MDA-MB-231 (Fig. 4G) and HeLa (Fig. 4H) cells, which are important down-stream effectors for tumor suppression effect of P53. All these data indicated that FTO inhibitor 18097 can modulate transcriptome and genes involved in P53 pathway of cancer cells.

3.5. SOCS1 was involved in FTO inhibitor-suppressed malignancy of cancer cells

Results showed that treatment with 18097 can positively regulate P53 pathway, which regulates genes involved in growth arrest, senescence, or cell apoptosis[34]. Among the 44 genes involved in P53 pathways and significantly regulated by 18097, we identified the only candidate, *SOCS1*, that overlapping among the top 50 upregulated genes in 18097-treated cells (Fig. 5A and Table S2). SOCS1 can directly interact with P53, which leads to activation of its transcriptional program and induction of cellular apoptosis, ferroptosis and senescence[35]. Western blot analysis confirmed that treatment of 18097 increased protein expression of SOCS1 and P53 in cancer cells (Fig. 5B). Consistently, si-FTO also increased mRNA (Fig. 5C) and protein (Fig. 5D) expression of SOCS1 in both MDA-MB-231 and HeLa cells. However, si-FTO can abolish 18097-induced mRNA expression of SOCS1 (Supporting Information Fig. S5B), which suggested that FTO is the effector for 18097-regulated expression of SOCS1.

TP53/SOCS1 axis was critical for EMT and growth of cancer cells[36,37]. In order to evaluate whether TP53/SOCS1 axis was involved in FTO inhibitor-suppressed malignancy of cancer cells, expression of *SOCS1* was knocked down by use of its specific siRNA (Fig. S5A). Results showed that si-*SOCS1* abolished 18097-suppressed migration (Fig. 5E) and invasion (Fig. 5F) of MDA-MB-231 cells. Consistently, si-*SOCS1* attenuated 18097-suppressed expression of FN in cancer cells (Fig. 5G). It confirmed that SOCS1 is involved in FTO inhibitor-suppressed malignancy of cancer cells.

Mechanisms responsible for 18097-regulated expression of *SOCS1* were further studied. m^{6}A-RIP-qPCR confirmed significant m^{6}A enrichment of *SOCS1* mRNA in MDA-MB-231 and HeLa cells, further, the m^{6}A enrichment of *SOCS1* mRNA increased in cells treated with 18097 (Fig. 5H and Fig. S5C). However, expression of precursor-*SOCS1* in cells treated with 18097 had no significant variation (Fig. S5D). Further, treatment

of 18097 had no significant effect on stability of precursor-*SOCS1* in MDA-MB-231 cells (Fig. S5E). It indicated that transcription and splicing of *SOCS1* may be independent to FTO. However, 18097 significantly increased mRNA stability of *SOCS1* in MDA-MB-231 cells (Fig. 5I). Consistently, over-expression of FTO decreased half-life of *SOCS1* mRNA in MDA-MB-231 (Fig. 5J). It indicated that FTO inhibitor 18097 can increase stability of *SOCS1* mRNA to elevate its expression.

IGF2BPs, HuR, and YTHDF1 can bind with the methylated RNA to regulate mRNA stability[38]. RIP-PCR showed that *SOCS1* can significantly bind with IGF2BP1, and the binding between *SCOS1* with IGF2BP1 was increased in MDA-MB-231 cells treated with 18097 (Fig. 5K). We further knocked down the expression of IGF2BP1 in MDA-MB-231 cells (Fig. S5F). si-*IGF2BP1* can decrease mRNA (Fig. 5L) and protein (Fig. 5M) of *SOCS1* in MDA-MB-231 and HeLa cells. It should be due to that si-*IGF2BP1* can decrease mRNA stability of *SOCS1* in MDA-MB-231 cells (Fig. 5N). Further, si-*IGF2BP1* can attenuate 18097-induced mRNA (Fig. 5O) and protein (Fig. 5P) expression of *SOCS1* in MDA-MB-231 cells. Collectively, 18097 can increase the stability of *SOCS1* mRNA *via* IGF2BP1.

3.6. FTO inhibitor suppressed cellular lipogenesis

FTO can trigger adipogenesis *in vivo* and induce lipid accumulation[39,40]. We further investigated roles of lipogenesis in 18097-inhibited cancer progression since lipid metabolism is critical for cancer development[41]. GSEA revealed that 18097-altered gene expression profile was positively associated with intermembrane lipid transporter activity while negatively associated with long chain fatty acid transporter activity (Fig. 6A and B), suggesting that treatment with 18097 may also regulate cellular lipogenesis. We then established a model of cellular lipogenesis by induction of preadipocytes to be adipocytes. Treatment with 18097 significantly decreased neutral lipid accumulation of 3T3-L1, HeLa and MDA-MB-231 cells (Fig. 6C). Effects of FTO inhibitor on fatty acid oxidation (FAO) functions of cancer cells were further checked. Results showed that treatment with 18097 can significantly suppress fatty acid (FA) uptake (Fig. 6D) and FAO rate (Fig. 6E) of cancer cells.

PPARγ, *C/EBPα/β,* and *ADD1* are key genes involved in FA metabolic[42]. We found that treatment with 18097 significantly decreased expression of *PPARγ* and *C/EBPα/β* in MDA-MB-231 (Fig. 6F) and HeLa (Supporting Information Fig. S6A) cells. Further, treatment with 18097 significantly decreased protein expression of PPARγ and C/EBPα/β in cancer cells (Fig. 6G). In addition, we found that the inhibitor can increase m6A of *PPARγ*, *C/EBPα*, and *C/EBPβ* mRNA in MDA-MB-231 (Fig. 6H) and HeLa (Supporting Information Fig. S6B) cells. Considering that previous study indicated that m6A can facilitate mRNA degradation, we also detected mature mRNA half-time by using Act-D to block transcription. Results showed that treatment with 18097 can significantly decrease mRNA half-time of *PPARγ*, *C/EBPα*, and *C/EBPβ* in MDA-MB-231 cells (Fig. 6I). Consistently, si-FTO also decreased mRNA expression (Fig. S6C) and mRNA half-time (Fig. S6D) of *PPARγ*, *C/EBPα*, and *C/EBPβ* in MDA-MB-231 cells. It might be due to that treatment with 18097 can significantly increase the binding between YTHDF2 with *PPARγ*, *C/EBPα*, and *C/EBPβ* in MDA-MB-231 cells (Fig. 6J). Therefore, results indicated that FTO inhibited the malignancy of tumor cells by suppression of adipogenesis.

3.7. Effects of FTO and 18097 on in vivo progression of breast cancer

We further examined the *in vivo* effects of FTO inhibitor by treating MDA-MB-231 xenograft with vehicle or 18097. Results showed that tumor size and volume of xenografts in 18097-injected group were significantly lower than that in control group (Fig. 7A), while treatment with 18097 had no significant effect on body weight (Supporting Information Fig. S7A). Ki67-positive staining was used to recognize a nuclear antigen expressed in proliferating cells, which was significantly decreased in the 18097 group (Fig. 7B). Further, treatment with 18097 can significantly increase expression of SOCS1, while decrease expression of PPARγ in xenograft tissues (Fig. 7B). Lung colonization model was generated by injection of MDA-MB-231^LMF3 cells into the lateral tail vein to evaluate effect of 18097 on *in vivo* cancer progression[28,31]. As shown in Fig. 7C–E, treatment with 18097 significantly decreased the number and size of lung tumors derived from MDA-MB-231^LMF3 cells. It indicated that targeted inhibition of FTO decreased *in vivo* growth and lung colonization of breast cancer cells.

Clinical data from Oncomine suggested that the expression of FTO in breast cancer tumor tissues was significantly increased as compared with that in normal tissues of Finak Breast (Fig. S7B). The effect of FTO on recurrence-free survival rate (RFS) was checked by Kaplan−Meier plotter[43]. It showed BC patients with increased expression of FTO had significantly reduced RFS (Fig. S7C). While BC patients with increased expression of SOCS1 had significantly increased RFS (Fig. S7D). In addition, we found that expression of FTO and *SOCS1* in 880 BC patients were negatively correlated (Fig. S7E, $P < 0.05$) based on data from LinkedOmics[44]. In addition, patients with increased FTO levels in tumor tissues of bladder, head-neck, lung and gastric cancer (Fig. S7F−I) showed significantly reduced RFS. Together, these results suggested the oncogenic roles of FTO in cancer development.

4. Discussion

Recent studies indicated that FTO contributed to the development of various cancers including AMLs, cervical, lung, melanoma and breast cancer to regulate initiation, progression, and drug resistance of cancer cells[11,13]. Previous studies reported a few FTO biochemical inhibitors to date[38]. The specific and high efficiency inhibitors to target FTO for cancer, specifically for solid tumors, are urgently needed. Our present study provided a potent and high specific FTO inhibitor-18097 by *in silico* virtual screening and validation assays. 18097 possibly occupies the catalytic pocket of FTO, thus effectively inhibits *in vitro* demethylation activity of FTO with the IC50 values of 0.64 μmol/L. The discovery of 18097 and its suppression effect on solid cancer would provide a potent inhibitor for research of RNA methylation on cancer pression and drug development.

Although several inhibitors such as rhein, MO-I-500, meclofenamic acid (MA), R-2HG, fluorescein, FB23-2, and entacapone can suppress the activities of FTO[11,18−24], only few shows cellular activities. We found that the inhibitor targeting FTO impaired cellular demethylation and caused significant biological impacts. Specifically, 18097 can hinder the migration, invasion, EMT potential and colonization of cancer cells and increase chemosensitivity to therapy drugs. *In vivo* data confirmed that 18097

significantly suppressed the lung metastasis of breast cancer cells, thus suggesting that FTO might serve as a potential target to suppress *in vivo* cancer metastasis. Cancer metastasis accounts for 90% of cancer-associated deaths[45]. Urgent research works are needed to confirm whether 18097 had similar effect to inhibit cancer metastasis beside breast cancer. In addition, the preclinical primary safety evaluation and pharmacokinetic properties of 18097 are also urgently needed.

We found that FTO/SOCS1 axis is important for m^{6}A regulated cancer progression. Previous studies indicated that SOCS1 was critical for EMT and growth of cancer cells[36,37]. Our inhibitor increased expression of SOCS1 by increasing its mRNA stability. Knockdown of *SOCS1* can attenuate 18097-suppressed migration, invasion and EMT potential of cancer cells. Both *in vitro* and *in vivo* results confirmed that SOCS1 is involved in FTO inhibitor-suppressed malignancy of cancer cells. Intriguingly, 18097 can increase the mRNA stability of *SOCS1* while decrease stability of *PPARG*, *CEBPA*, and *CEBPB*, which might be due to the difference of binding readers. The mechanisms need further explorations with a more depth.

Although FTO has been implicated in obesity for a long time[9,46], our present study found that 18097 had no significant effect on body weight of mice. It suggested that whether FTO is a valid drug target for body weight control remains ambiguous. However, our data indicated that 18097 can suppress adipogenesis of cancer cells *via* suppressing FA uptake and oxidation. Specifically, 18097 can decrease expression of *PPARγ* and *C/EBPα/β via* decreasing their mRNA stability. Consistently, previous studies indicated that FTO knockdown reduces the mRNA stability of PPARγ *via* YTHDF2 involvement[47]. Specifically, FTO bound with and then demethylated PPARγ mRNA, leading to upregulation of PPARγ mRNA[48]. FTO can trigger the adipogenesis *in vivo* and induce lipid accumulation[39,40]. The *PPARγ* and members of the *C/EBP* family are important regulators for adipogenesis and lipid storage[49]. Adipogenesis is essential for cancer initiation and development including growth, metastasis, and angiogenesis[50]. The essential roles of adipogenesis in 18097-suppressed cancer metastasis need further investigations.

5. Conclusions

Our present study developed 18097, a specific and potent FTO inhibitor, to suppress malignancy of solid tumor cells both *in vitro* and *in vivo*, particularly for its inhibitory effect on *in vivo* metastasis of breast cancer cells. It suggested FTO can work as a potential drug target and small-molecule inhibitor 18097 can serve as a potential agent against breast cancer.

Author contributions

Guoyou Xie: data curation, writing-original draft preparation, validation; Xu-Nian Wu and Yuyi Ling: data curation, writing-original draft preparation, investigation; Yalan Rui: data curation, writing-original draft preparation, software, validation; Deyan Wu: supervision, data curation; Jiawang Zhou: data curation, validation; Jiexin Li: software, validation; Shuibin Lin, Qing Peng and Ziang Li: supervision, data curation; Hai-Bin Luo and Hongsheng Wang: conceptualization, supervision, writing-reviewing and editing.

Conflicts of interest

The authors declare no conflict of interest.

Appendix A.   Supporting information

Supporting information to this article can be found online at https://doi.org/10.1016/j.apsb.2021.08.028.

References

1. Wei CM, Gershowitz A, Moss B. Methylated nucleotides block 5′ terminus of HeLa cell messenger RNA. *Cell* 1975;**4**:379−86.
2. Wei CM, Gershowitz A, Moss B. 5′-Terminal and internal methylated nucleotide sequences in HeLa cell mRNA. *Biochemistry* 1976;**15**: 397−401.
3. Roundtree IA, Evans ME, Pan T, He C. Dynamic RNA modifications in gene expression regulation. *Cell* 2017;**169**:1187−200.
4. Jia G, Fu Y, Zhao X, Dai Q, Zheng G, Yang Y, et al. N^6-Methyladenosine in nuclear RNA is a major substrate of the obesity-associated FTO. *Nat Chem Biol* 2011;**7**:885−7.
5. Zheng G, Dahl JA, Niu Y, Fedorcsak P, Huang CM, Li CJ, et al. ALKBH5 is a mammalian RNA demethylase that impacts RNA metabolism and mouse fertility. *Mol Cell* 2013;**49**:18−29.
6. Liu J, Yue Y, Han D, Wang X, Fu Y, Zhang L, et al. A METTL3-METTL14 complex mediates mammalian nuclear RNA N^6-adenosine methylation. *Nat Chem Biol* 2014;**10**:93−5.
7. Yue Y, Liu J, He C. RNA N^6-methyladenosine methylation in post-transcriptional gene expression regulation. *Genes Dev* 2015;**29**:1343−55.
8. Chen XY, Zhang J, Zhu JS. The role of m^{6}A RNA methylation in human cancer. *Mol Cancer* 2019;**18**:103.
9. Frayling TM, Timpson NJ, Weedon MN, Zeggini E, Freathy RM, Lindgren CM, et al. A common variant in the *FTO* gene is associated with body mass index and predisposes to childhood and adult obesity. *Science* 2007;**316**:889−94.
10. Han Z, Niu T, Chang J, Lei X, Zhao M, Wang Q, et al. Crystal structure of the FTO protein reveals basis for its substrate specificity. *Nature* 2010;**464**:1205−9.
11. Su R, Dong L, Li C, Nachtergaele S, Wunderlich M, Qing Y, et al. R-2HG exhibits anti-tumor activity by targeting FTO/m^{6}A/MYC/CEBPA signaling. *Cell* 2018;**172**:90−105.e123.
12. Wei J, Liu F, Lu Z, Fei Q, Ai Y, He PC, et al. Differential m^{6}A, m^{6}Am, and m^{1}A demethylation mediated by FTO in the cell nucleus and cytoplasm. *Mol Cell* 2018;**71**:973−985 e975.
13. Li Z, Weng H, Su R, Weng X, Zuo Z, Li C, et al. FTO plays an oncogenic role in acute myeloid leukemia as a N^6-Methyladenosine RNA demethylase. *Cancer Cell* 2017;**31**:127−41.

14. Cui Q, Shi H, Ye P, Li L, Qu Q, Sun G, et al. m6A RNA methylation regulates the self-renewal and tumorigenesis of glioblastoma stem cells. *Cell Rep* 2017;**18**:2622−34.

15. Yang S, Wei J, Cui YH, Park G, Shah P, Deng Y, et al. m6A mRNA demethylase FTO regulates melanoma tumorigenicity and response to anti-PD-1 blockade. *Nat Commun* 2019;**10**:2782.

16. Niu Y, Lin Z, Wan A, Chen H, Liang H, Sun L, et al. RNA N^6-methyladenosine demethylase FTO promotes breast tumor progression through inhibiting BNIP3. *Mol Cancer* 2019;**18**:46.

17. Zhao J, Lu L. Interplay between RNA methylation eraser FTO and writer METTL3 in renal clear cell carcinoma patient survival. *Recent Pat Anticancer Drug Discov* 2021;**16**:363−76.

18. Chen B, Ye F, Yu L, Jia G, Huang X, Zhang X, et al. Development of cell-active N^6-methyladenosine RNA demethylase FTO inhibitor. *J Am Chem Soc* 2012;**134**:17963−71.

19. He W, Zhou B, Liu W, Zhang M, Shen Z, Han Z, et al. Identification of a novel small-molecule binding site of the fat mass and obesity associated protein (FTO). *J Med Chem* 2015;**58**:7341−8.

20. Huang Y, Yan J, Li Q, Li J, Gong S, Zhou H, et al. Meclofenamic acid selectively inhibits FTO demethylation of m6A over ALKBH5. *Nucleic Acid Res* 2015;**43**:373−84.

21. Huang Y, Su R, Sheng Y, Dong L, Dong Z, Xu H, et al. Small-molecule targeting of oncogenic FTO demethylase in acute myeloid leukemia. *Cancer Cell* 2019;**35**: 677−91.e610.

22. Peng S, Xiao W, Ju D, Sun B, Hou N, Liu Q, et al. Identification of entacapone as a chemical inhibitor of FTO mediating metabolic regulation through FOXO1. *Sci Transl Med* 2019;**11**:eaau7116.

23. Wang T, Hong T, Huang Y, Su H, Wu F, Chen Y, et al. Fluorescein derivatives as bifunctional molecules for the simultaneous inhibiting and labeling of FTO protein. *J Am Chem Soc* 2015;**137**:13736−9.

24. Toh JDW, Sun L, Lau LZM, Tan J, Low JJA, Tang CWQ, et al. A strategy based on nucleotide specificity leads to a subfamily-selective and cell-active inhibitor of N^6-methyladenosine demethylase FTO. *Chem Sci* 2015;**6**:112−22.

25. Su R, Dong L, Li Y, Gao M, Han L, Wunderlich M, et al. Targeting FTO suppresses cancer stem cell maintenance and immune evasion. *Cancer Cell* 2020;**38**:79−96.e11.

26. Wu Y, Wang Q, Jiang MY, Huang YY, Zhu Z, Han C, et al. Discovery of potent phosphodiesterase-9 inhibitors for the treatment of hepatic fibrosis. *J Med Chem* 2021;**64**:9537−49.

27. Yang CG, Yi C, Duguid EM, Sullivan CT, Jian X, Rice PA, et al. Crystal structures of DNA/RNA repair enzymes AlkB and ABH2 bound to dsDNA. *Nature* 2008;**452**:961−5.

28. Lu L, Chen Z, Lin X, Tian L, Su Q, An P, et al. Inhibition of BRD4 suppresses the malignancy of breast cancer cells *via* regulation of Snail. *Cell Death Differ* 2020;**27**:255−68.

29. Liu C, Liu R, Zhang D, Deng Q, Liu B, Chao HP, et al. MicroRNA-141 suppresses prostate cancer stem cells and metastasis by targeting a cohort of pro-metastasis genes. *Nat Commun* 2017;**8**:14270.

30. Chen ZJ, Wu L, Zhou JW, Lin X, Peng YX, Ge LC, et al. N^6-methyladenosine-induced ERRγ triggers chemoresistance of cancer cells through upregulation of ABCB1 and metabolic reprogramming. *Theranostics* 2020;**10**:3382−96.

31. Lin X, Chai G, Wu Y, Li J, Chen F, Liu J, et al. RNA m6A methylation regulates the epithelial mesenchymal transition of cancer cells and translation of Snail. *Nat Commun* 2019;**10**:2065.

32. Li Z, Cai YH, Cheng YK, Lu X, Shao YX, Li X, et al. Identification of novel phosphodiesterase-4D inhibitors prescreened by molecular dynamics-augmented modeling and validated by bioassay. *J Chem Inf Model* 2013;**53**:972−81.

33. Kanehisa M, Sato Y, Kawashima M, Furumichi M, Tanabe M. KEGG as a reference resource for gene and protein annotation. *Nucleic Acid Res* 2016;**44**:D457−62.

34. Levine AJ. p53: 800 million years of evolution and 40 years of discovery. *Nat Rev Cancer* 2020;**20**:471−80.

35. Lessard F, Saint-Germain E, Mignacca L, Ferbeyre G. SOCS1: phosphorylation, dimerization and tumor suppression. *Oncoscience* 2019;**6**:386−9.

36. Jackson-Weaver O, Ungvijanpunya N, Yuan Y, Qian J, Gou Y, Wu J, et al. PRMT1-p53 pathway controls epicardial EMT and invasion. *Cell Rep* 2020;**31**:107739.

37. Chang CJ, Chao CH, Xia WY, Yang JY, Xiong Y, Li CW, et al. p53 regulates epithelial−mesenchymal transition and stem cell properties through modulating miRNAs. *Nat Cell Biol* 2011;**13**. 317-U296.

38. Huang H, Weng H, Chen J. m6A modification in coding and non-coding RNAs: roles and therapeutic implications in cancer. *Cancer Cell* 2020;**37**:270−88.

39. Merkestein M, Laber S, McMurray F, Andrew D, Sachse G, Sanderson J, et al. FTO influences adipogenesis by regulating mitotic clonal expansion. *Nat Commun* 2015;**6**:6792.

40. Church C, Moir L, McMurray F, Girard C, Banks GT, Teboul L, et al. Overexpression of Fto leads to increased food intake and results in obesity. *Nat Genet* 2010;**42**:1086−92.

41. Snaebjornsson MT, Janaki-Raman S, Schulze A. Greasing the wheels of the cancer machine: the role of lipid metabolism in cancer. *Cell Metabol* 2020;**31**:62−76.

42. Grimaldi PA. The roles of PPARs in adipocyte differentiation. *Prog Lipid Res* 2001;**40**:269−81.

43. Szasz AM, Lanczky A, Nagy A, Forster S, Hark K, Green JE, et al. Cross-validation of survival associated biomarkers in gastric cancer using transcriptomic data of 1,065 patients. *Oncotarget* 2016;**7**: 49322−33.

44. Vasaikar SV, Straub P, Wang J, Zhang B. LinkedOmics: analyzing multi-omics data within and across 32 cancer types. *Nucleic Acids Res* 2018;**46**:D956−63.

45. Lambert AW, Pattabiraman DR, Weinberg RA. Emerging biological principles of metastasis. *Cell* 2017;**168**:670−91.

46. Claussnitzer M, Dankel SN, Kim KH, Quon G, Meuleman W, Haugen C, et al. FTO obesity variant circuitry and adipocyte browning in humans. *N Engl J Med* 2015;**373**:895−907.

47. Gu XF, Zhang YW, Li D, Cai HS, Cai LH, Xu Q. N^6-methyladenosine demethylase FTO promotes M1 and M2 macrophage activation. *Cell Signal* 2020;**69**:109553.

48. Shen GS, Zhou HB, Zhang H, Chen B, Liu ZP, Yuan Y, et al. The GDF11-FTO-PPAR gamma axis controls the shift of osteoporotic MSC fate to adipocyte and inhibits bone formation during osteoporosis. *BBA-Mol Basis Dis* 2018;**1864**:3644−54.

49. Farmer SR. Transcriptional control of adipocyte formation. *Cell Metabol* 2006;**4**:263−73.

50. Wu R, Wang X. Epigenetic regulation of adipose tissue expansion and adipogenesis by N^6-methyladenosine. *Obes Rev* 2021;**22**:e13124.